Shear Wave Elastography Combined with Molecular Subtype in Early Predicting Response to Neoadjuvant Chemotherapy for Breast Cancer: A Prospective Case-control Study

Jia-Xin Huang
Sun Yat-sen University Cancer Center https://orcid.org/0000-0002-8038-0175
Shi-Yang Lin
Guangzhou Medical College First Affiliated Hospital
Yan Ou
The Seventh Affiliated Hospital Sun Yat-sen University
Cai-Gou Shi
Liuzhou People's Hospital
Yuan Zhong
Sun Yat-sen University Cancer Center
Ming-Jie Wei
Sun Yat-sen University Cancer Center
Xiao-Qing Pei (peixq@sysucc.org.cn)
Sun Yat-sen University Cancer Center https://orcid.org/0000-0002-6832-1228

Research article

Keywords: Breast cancer, Neoadjuvant chemotherapy, Early prediction, Pathological response, Quantitative shear wave elastography

Posted Date: June 18th, 2021

DOI: https://doi.org/10.21203/rs.3.rs-600929/v1

Abstract

Background: This study was designed to investigate the performance of quantitative shear wave elastography (SWE) and the accuracy of SWE with the molecular subtype for early prediction of pathological response of breast cancer to neoadjuvant chemotherapy (NAC).

Methods: In this prospective case-control study, 102 patients were screened from September 2016 to August 2020. Characteristics of conventional ultrasonography (US), SWE and contrast-enhanced magnetic resonance imaging (CE-MRI), were recorded, and the changes were compared to the pre-NAC baseline data. The pathological response was classified according to the Miller Payne grading system. Multivariate logistic regression was used to develop a predictive model for the response to NAC.

Results: Significant differences related to changes in SWE characteristics of breast lesions between between pathological response groups were observed earlier than size on the conventional US and MRI images. According to the multivariate predictive model, the best parameter for predicting the pathological response after the first cycle of NAC was the molecular subtype of the tumor [area under the curve (AUC) = 0.83] with low sensitivity (66.04%). Better predictive performance was achieved when $\triangle A_{E/B}$ and the molecular subtype were applied in combination after the second cycle of NAC (AUC = 0.92) with a higher sensitivity (86.79%). The predictive performance of molecular subtype combined with $\triangle A_{E/B}$ and $\triangle SWV_{mean}$ after the third and fourth cycles of NAC were improved (AUC = 0.94).

Conclusion: The SWE can be an early predictor of the pathological response to NAC for breast cancer. The combination of SWE and the molecular subtype may be a preferred method for the clinical evaluation of NAC to facilitate the personalization of treatment regimens for breast cancer.

Introduction

Breast cancer is the most common malignant tumor and the most frequent cause of tumor-related mortality in women worldwide.[1] Neoadjuvant chemotherapy (NAC) followed by mastectomy is one of the most important parts of breast cancer therapy. NAC can be used as an in vivo chemosensitivity test, which enables the evaluation of chemotherapy. Moreover, NAC has other advantages such as reducing the tumor burden and downstaging cancer to increase the chances of surgery or breast-conserving surgery. NAC has also been reported to reduce the need for axillary lymph node dissection (ALND) and prevent micro-metastasis during surgery in a previous study.[2 3] However, patients with chemotherapy resistance cannot benefit from NAC and may suffer from adverse reactions due to unnecessary chemotherapy. Furthermore, the timing of the operation may be delayed. Although a large number of clinical trials have shown that NAC is effective for treating breast cancer, studies have also indicated that its efficacy is variable. Previous investigations demonstrated that the overall response rates for NAC range from 69–100%, with pathological complete response (pCR) from 10–15% of patients.[4] Therefore, a

practical approach for the early evaluation and prediction of the patient response to NAC is of great importance for the optimization of therapy in clinical practice.

In clinical practice, traditional imaging, including mammography, ultrasound (US), magnetic resonance imaging (MRI), and positron emission tomography (PET), coupled with physical examination is the primary method to evaluate the NAC response. However, the performance of mammography alone for predicting the pathological response to NAC is limited.[5–7] MRI, PET, and other emerging techniques are time-consuming, expensive, and contraindicated for some patients.[8–13] Therefore, there is no consensus approach for evaluating the response to NAC in patients with breast cancer during chemotherapy.

As a convenient, real-time, low-cost, and non-invasive imaging approach, US is superior for wide utilization for the evaluation of NAC for breast cancer.[5–7] Patients with breast cancer were recommended to be re-evaluated for NAC response regularly using US after each two cycles of NAC according to the China Anti-Cancer Association breast cancer guideline.[14] And several studies have shown that US and MRI display similar performance in evaluating the response to NAC.[15 16] However, the accuracy of conventional US is limited for monitoring changes in tumors during NAC.[5–7 13]

Ultrasound Elastography (UE) is an emerging imaging method based on biomechanical properties that can be used to diagnose breast lesions and assess breast cancer therapy.[17] Elastosonography, including strain elastography (SE) and shear wave elastography (SWE), was performed in this study according to the guidelines and recommendations for elastography presented by the World Federation of Ultrasound in Medicine and Biology (WFUMB).[18] NAC can cause microscopic pathological changes such as tumor cell apoptosis and fibrosis, altering the bio-mechanical properties of tumor tissues.[19 20] Initial studies have shown that SE can be utilized to differentiate patients who respond or do not respond to NAC by assessing the macroscopic structures of the tumor tissues.[18] Yan *et al.* demonstrated that SWE exhibited better performance than SE for predicting NAC resistance.[21]

SWE is a quantitative and objective modality for assessing changes in the biomechanical characteristics of a tumor.[22] Therefore, it is expected to achieve clinical application for the evaluation of NAC for breast cancer. There has been relatively little research on the differences between SWE and conventional imaging methods or investigations on the performance of SWE with clinicopathological factors for predicting the early response to NAC for breast cancer. The present study was an endeavor to evaluate SWE's performance in predicting the pathological response to NAC in patients with breast cancer compared to conventional US and MRI based on tumor morphological changes. Furthermore, the study was aimed at generating a multi-factor prediction model using imaging and clinicopathological factors in a new predictive modality to obtain additional information for the development of individualized therapy regimens.

Materials And Methods

The present study was a prospective case-control study. The study's design and protocol were approved by the ethics committee of the institutional review board at the Cancer Center of Sun Yat-Sen University (approval GZR2017-047). Written informed consent for study participation and data collection were obtained from all patients.

Patients and Study Procedure

Patients were consecutively recruited at the Cancer Center of Sun Yat-Sen University (Guangdong, China) between October 2016 and August 2020. The inclusion criteria were: (i) the patients had invasive breast cancer confirmed with US-guided core needle biopsy, without distant metastasis; (ii) the patients received eight cycles of a standardized NAC regimen; (iii) the patients had at least one targeted measurable lesion according to RECIST 1.1,[23] and (iv) surgery was conducted after completion of NAC. The exclusion criteria were: (i) patients who did not complete full course of NAC as intolerance to chemotherapy, (ii) tumor progression, leading to palliative chemoradiotherapy instead of surgery, (iii) lesion size exceeding the scope of a color-coded map in the assessment view of SWE, and (iv) low-quality data in quantitative SWE with a large area of elasticity defects on the SWE velocity image.

Each included patient was continuously followed up with US and MRI before the surgery. US examinations, including conventional US and SWE, were performed one day before the biopsy (time point t0) and one day before the second (t1), third (t2), fourth (t3), and fifth cycles (t4) of NAC (time point t1-t4). MRI examinations were performed before the biopsy and within 3 days before the fifth cycle of NAC (time point t4). Surgical excision was performed approximately 2 weeks after eight cycles of NAC. The flow chart depicting the study design is shown in Fig. 1.

NAC regimen

NAC strategies were performed according to the standard protocol at our institution. All patients received eight cycles of chemotherapy based on anthracycline/taxane. Moreover, patients with positive HER-2 expression received trastuzumab, starting from the fifth cycle of NAC.

Related examinations

B-mode US and SWE images were obtained with the Siemens S2000 ultrasound system (Siemens Medical Solutions, Mountain View, CA, USA) equipped with a 9L4 linear transducer. Conventional US and SWE images of breast lesions were acquired with patients in the supine position according to the breast US examination guideline from the American Institute of Ultrasound in Medicine.[24] Firstly, conventional US scans were performed to locate the breast lesions and obtain greyscale and color Doppler flow images. The longest diameter (D_{US}) and area (A_B) of the breast lesion on the B-mode image were recorded. Secondly, SWE was performed at the same position, depth, focus position, and gain setting used for conventional US scanning. Furthermore, a probe was held still and applied perpendicular to the skin with the minimum amount of pressure possible. SWE was performed by setting the region of interest (ROI) for stiffness assessment to include the breast tumors and surrounding normal tissue. SWE was

performed with the patients holding their breath for approximately 5 seconds. A quality map displayed in green-yellow-red indicating high-intermediate-low quality was obtained first to evaluate the Shear Wave Velocity (SWV). Next, the image was switched to the SWV map, which was displayed in color mode to indicate the stiffness ranging from soft (blue) to intermediate (green or yellow) and hard (red). The part corresponding to high SW quality (green areas on the quality map) was selected for the measurement of the SWV to ensure SWE reliability. Within the ROI, SWV values ranging from 0.5 to 10 m/s on the velocity map were obtained by placing three SWV-ROIs (2×2 mm) over the lesion's stiffest and softest parts, respectively. Finally, the image was switched to a Shear Wave Time (SWT) map, and the profile of the breast lesion was delineated to measure the area of the lesion (A_E) according to the color-coded differences between the tumor and the surrounding tissues.

The US examinations were conducted by two board-certified radiologists (Jia-Xin Huang and Shi-Yang Lin) with at least 2 years of experience in the performance and interpretation of breast US, as well as at least 6 months of experience in performing elastography before the onset of this study. SWE images were reviewed and confirmed to be eligible by a third radiologist (Xiao-Qing Pei) who had 20 years of experience in ultrasonography and 5 years of experience in breast elastography imaging. The US examination and measurement procedures are shown in Fig. 2.

All breast MRI examinations were performed on an eight-channel 3.0-T system (Discovery MR750, GE Medical Systems, Milwaukee, WI, USA). Patients were imaged in the head-first prone position, and images were obtained with bilateral axial views. Images were interpreted by radiologists with more than 5 years of experience with MRI of the breast. Measurements of the maximal diameter (D_{MRI}) of breast cancer were obtained on post-contrast subtracted T1-weighted images.

Imaging Parameters Calculation

The maximal and minimal values of SWV (SWV_{max} and SWV_{min}) were recorded by averaging three measured values, respectively. The mean SWV values (SWV_{mean}) for the six SWV-ROIs were calculated.[25] Additionally, the area ratio ($A_{E/B}$) was calculated as the ratio of the area of the breast tumor in the SWE time image to that in the B-mode screen. The relative changes of the breast lesion [Δ values (%)] in the B-mode US, SWE, and MRI images were calculated at each time point. The equations used to calculate these parameters can be found in Appendix A.

Pathological evaluation

All pathological results were determined by two board-certified pathologists with consensus who were blinded to the imaging information for the patients.

Before the onset of NAC, the diagnosis was determined with a US-guided core needle biopsy. Samples from the core needle biopsy were examined to obtain the biological characteristics of the breast tumors.

The expression levels of estrogen receptor (ER), progesterone receptor (PR), human epidermal growth factor receptor 2 (HER2), and Ki-67 in core needle biopsy specimens were evaluated with immunohistochemistry (IHC) and fluorescence in situ hybridisation (FISH). The criteria for the IHC, FISH and molecular subtype results were determined according to the St. Gallen consensus.[26–30]

After eight cycles of NAC, all patients received mastectomy along with ALND or sentinel lymph node biopsy (SLNB). Assessment of the NAC response was performed using the Miller-Payne system as defined in Appendix B. A grade of 4 or 5 was categorized as a Major Histological Response (MHR) and a grade of 1, 2, or 3 was defined as a Non-major Histological Response (NMHR).

Data collection

Data on the demographics, IHC characteristics of breast cancer, breast tumor size/stage, lymph node stage, clinical stage, and pathological response grade of NAC were collected. During the chemotherapy follow-up, the maximum diameter of the breast tumor on the B-mode US, the maximum and average values of SWV, the ratio of tumor area on the elastic image to that on the B-mode US, and the maximum diameter of the breast tumor on the enhanced T1 MRI image were recorded.

Statistical analysis

Continuous data were presented as the mean and standard deviation (SD), and categorical variables were presented as counts. Univariate analysis for the pathological response was performed by using a *t*-test or Mann-Whitney *U* test to compare continuous quantitative variables between the responsive and non-responsive groups. The Kruskal-Wallis test, X^2 test, or Fisher exact test were used to compare the categorical variables in the two pathological response groups.

When both the imaging parameters and clinicopathological characteristics showed favorable efficiency in univariate analysis, we generated a multivariate regression model by using the factors with statistical significance to create a new predictive modality. A *p*-value of < 0.05 was entry probability for stepwise of multivariate logistic regression while a *p*-value of more than 0.10 was defined as removal probability. The receiver operating characteristic (ROC) curve was drawn to determine the performance of the imaging findings and combined parameters (CP) in predicting the pathological response.[32] An area under the ROC (AUC) value of > 0.9 indicated a great diagnostic value, $0.9 > \text{AUC} > 0.7$ suggested a moderate diagnostic value, and $\text{AUC} < 0.7$ was considered to indicate a poor diagnostic value.[32] The cut-off point for these features was determined by maximizing the Youden coefficient.[33] A p-value of < 0.05 was considered to indicate statistical significance. Data analysis was performed with the Statistical Package for the Social Sciences (SPSS) version 22.0 and Medical Statistical Software version 16.2.

Results

Patient clinical and pathological characteristics

A total of 102 patients with confirmed invasive breast cancer who received NAC were screened. Finally, 80 cases were enrolled according to the eligibility criteria. The mean age (mean ± standard deviation) of the included patients was 46.41 ± 10.56 years. Most of the patients (64/80) had clinical TNM stage III tumor and 16 patients had stages II tumor. The most frequent molecular subtype was Luminal B1 (45.00%, 36/80).

27 included patients (33.75%, 27/80) were classified as MHR, while 66.25% (53/80) patients presented NMHR after eight cycles of NAC. No statistically significant differences were observed for other clinical and pathological characteristics between the two pathological response groups except for the molecular subtype. The clinical and pathological characteristics are shown in Table 1.

Table 1
The clinical and pathological characteristics at baseline

Clinical and pathological Characteristics	All included Patients (n = 80)	Patients with MHR (n = 27)	Patients with NMHR (n = 53)	*p*-value
Age	46.41 ± 10.56	45.46 ± 10.17	46.92 ± 10.82	0.64
Tumor stage				0.42
1	10	3	7	
2	41	14	27	
3	15	3	12	
4	14	7	7	
Nodal status				0.53
0	4	0	4	
1	20	6	14	
2	27	11	16	
3	29	10	19	
Clinical stage				0.56
I	0	0	0	
II	16	4	12	
III	64	23	41	
IV	0	0	0	
Molecular subtype				< 0.01
Luminal A	2	1	1	
Luminal B1	36	1	35	
Luminal B2	26	15	11	
Her2-positive	11	6	5	
Triple negative	5	4	1	

Abbreviation: MHR, Major Histological Response; NMHR, Non-major Histological Response; HER2, human epidermal growth factor receptor 2.

Imaging parameters evaluation

There were no statistically significant differences in pre-treatment imaging measurements, including the observed values in conventional US, SWE, and MRI between the two pathological response groups, as summarized in Table 2.

Table 2
The baseline imaging characteristics

Baseline Imaging characteristics	Patients in total (n = 80)	Patients with MHR (n = 27)	Patients with NMHR (n = 53)	*p*-value
$D_{US}0$(cm)	3.18 ± 1.47	3.11 ± 1.31	3.21 ± 1.56	0.76
$SWV_{max}0$(m/s)	7.32 ± 1.82	6.92 ± 1.87	7.52 ± 1.78	0.53
$SWV_{mean}0$(m/s)	6.11 ± 1.72	5.93 ± 1.81	6.20 ± 1.68	0.18
$A_{E/B}0$	1.51 ± 0.72	1.59 ± 0.88	1.47 ± 0.64	0.58
$D_{MRI}0$(cm)	3.98 ± 1.76	4.39 ± 1.60	3.84 ± 1.81	0.38
Values were given as mean ± standard deviation.				
Abbreviation: MHR, Major Histological Response; NMHR, Non-major Histological Response; D_{US}, longest diameter of tumor on the B-mode US; SWV_{max}, the maximum shear wave velocity; SWV_{mean}; the average shear wave velocity; $A_{E/B}$, area ratio of lesion on the shear wave time map to the B-mode US screen; D_{MRI}, longest diameter of tumor on the MR image				

Predictive diagnostic performance of imaging parameters

Over the course of NAC, all imaging values gradually decreased and declined more in good responders than in poor responders. However, the differences in $\triangle D_{US}$ and $\triangle D_{MRI}$ between good responders and poor responders were not statistically significant.

After the second, third, and fourth cycles of NAC, differences in the relative changes in the maximum SWV ($\triangle SWV_{max}$) compared to pre-treatment values were statistically significant between two response groups [MHR vs. NMHR (*p*-value): after the second cycle 37.94 ± 19.93 vs. 22.91 ± 23.30 (< 0.01); after the third cycle 43.55 ± 19.84 vs. 23.41 ± 25.59 (< 0.01); after the fourth cycle55.81 ± 15.05 vs. 29.26 ± 29.86 (< 0.01)]. Likewise, the changes in the average SWV measurements ($\triangle SWV_{mean}$) compared to the baseline between the two response groups started to present statistically significant differences after the second cycle of NAC [MHR vs. NMHR (*p*-value): after the second cycle 35.94 ± 17.99 vs. 20.75 ± 23.07 (< 0.01); after the third cycle 45.41 ± 16.83 vs. 20.83 ± 25.46 (< 0.01); after the fourth cycle 53.67 ± 015.23 vs. 26.27 ± 29.56 (< 0.01)].

Above all, there were significant differences related to changes in the ratio of the tumor area in the SWT map to B-mode US($\triangle A_{E/B}$) after each cycle of NAC in the early stage of chemotherapy [MHR vs. NMHR (p-value): after the first cycle 16.51 ± 45.09 vs. 1.34 ± 32.15 (0.02); after the second cycle 46.12 ± 48.36 vs.

7.78 ± 52.56 (< 0.01); after the third cycle 46.543 ± 52.51 vs. 7.91 ± 64.84 (< 0.01); after the fourth cycle 54.69 ± 59.99 vs. 11.23 ± 95.00 (< 0.01)]. The changes in all imaging measurements at each time point of examination during the early NAC course are listed in Table 3.

Table 3
The relative changes in imaging characteristics from baseline at each time point of examination.

The relative changes in imaging characteristics	Patients in total (n = 80)	Patients with MHR (n = 27)	Patients with NMHR (n = 53)	*p* value
$\triangle D_{US}(t1)(\%)$	6.69 ± 13.89	7.53 ± 11.69	6.26 ± 14.97	0.78
$\triangle D_{US}(t2)(\%)$	13.38 ± 17.01	16.86 ± 19.88	11.61 ± 15.24	0.19
$\triangle D_{US}(t3)(\%)$	19.15 ± 21.56	24.59 ± 27.18	16.38 ± 17.70	0.16
$\triangle D_{US}(t4)(\%)$	25.74 ± 25.37	30.89 ± 31.57	23.12 ± 21.41	0.26
$\triangle SWV_{max}(t1)(\%)$	17.89 ± 17.63	21.71 ± 16.73	15.95 ± 17.91	0.17
$\triangle SWV_{max}(t2)(\%)$	27.98 ± 23.22	37.94 ± 19.93	22.91 ± 23.30	< 0.01
$\triangle SWV_{max}(t3)(\%)$	30.21 ± 25.54	43.55 ± 19.84	23.41 ± 25.59	< 0.01
$\triangle SWV_{max}(t4)(\%)$	38.22 ± 28.65	55.81 ± 15.05	29.26 ± 29.86	< 0.01
$\triangle SWV_{mean}(t1)(\%)$	16.29 ± 16.83	20.59 ± 16.58	14.11 ± 16.69	0.10
$\triangle SWV_{mean}(t2)(\%)$	25.88 ± 22.56	35.94 ± 17.99	20.75 ± 23.07	< 0.01
$\triangle SWV_{mean}(t3)(\%)$	29.13 ± 25.63	45.41 ± 16.83	20.83 ± 25.46	< 0.01
$\triangle SWV_{mean}(t4)(\%)$	35.52 ± 28.66	53.67 ± 015.23	26.27 ± 29.56	< 0.01
$\triangle A_{E/B}(t1)(\%)$	6.46 ± 37.44	16.51 ± 45.09	1.34 ± 32.15	0.02
$\triangle A_{E/B}(t2)(\%)$	10.41 ± 56.97	46.12 ± 48.36	7.78 ± 52.56	< 0.01
$\triangle A_{E/B}(t3)(\%)$	10.46 ± 65.92	46.543 ± 52.51	7.91 ± 64.84	< 0.01
$\triangle A_{E/B}(t4)(\%)$	11.02 ± 90.05	54.69 ± 59.99	11.23 ± 95.00	< 0.01

Values were given as mean ± standard deviation

Abbreviation: MHR, Major Histological Response; NMHR, Non-major Histological Response; D_{us}, longest diameter of tumor on the B-mode US; SWV_{max}, the maximum shear wave velocity; SWV_{mean}; the average shear wave velocity; $A_{E/B,}$ the area ratio of a lesion on the shear wave time map to the B-mode US screen; D_{MRI}, longest diameter of tumor on the MR image.

The relative changes in imaging characteristics	Patients in total (n = 80)	Patients with MHR (n = 27)	Patients with NMHR (n = 53)	*p* value
$\triangle D_{MRI}(t4)(\%)$	0.28 ± 0.22	0.32 ± 0.24	0.25 ± 0.20	0.38
Values were given as mean ± standard deviation				
Abbreviation: MHR, Major Histological Response; NMHR, Non-major Histological Response; D_{us}, longest diameter of tumor on the B-mode US; SWV_{max}, the maximum shear wave velocity; SWV_{mean}; the average shear wave velocity; $A_{E/B,}$ the area ratio of a lesion on the shear wave time map to the B-mode US screen; D_{MRI}, longest diameter of tumor on the MR image.				

The AUC was obtained for conventional US, SWE, and MRI variables to determine the predictive diagnostic performance. $\triangle A_{E/B}$ after each cycle in the early stage of NAC had better performance for predicting pathological response compared to other imaging characteristics. After the first, second, third, and fourth cycles of NAC, the AUCs for $\triangle A_{E/B}$ for predicting the pathological response were 0.67, 0.83, 0.78, and 0.79, respectively. However, $\triangle A_{E/B}$ only showed moderate predictive diagnostic performance for the response to NAC.

Furthermore, the sensitivity of $\triangle A_{E/B}$ did not maintain high with enough specificity to meet the requirements for NAC evaluation. The performance changes in all imaging variables for predicting the pathological response to NAC after each NAC cycle are listed in Table 4. ROC curves for $\triangle A_{E/B}$ after each cycle of NAC for predicting the pathological response to chemotherapy are shown in Fig. 3. Representative dynamic changes in the breast tumor on MR, B-model US, and SWE images for one patient are presented in Fig. 5.

Table 4
Performance of relative changes in imaging characteristics for predicting response to NAC.

Relative changes in imaging characteristics	AUC	Sensitivity(%)	Specificity(%)	Youden index	Cut-off value(%)	*p* value
$\triangle D_{US}(t1)$	0.52	60.38	55.56	0.16	4.84	0.78
$\triangle D_{US}(t2)$	0.56	96.23	25.93	0.22	34.78	0.43
$\triangle D_{US}(t3)$	0.57	81.13	48.15	0.29	26.32	0.34
$\triangle D_{US}(t4)$	0.57	83.02	44.44	0.27	40.69	0.36
$\triangle SWV_{max}(t1)$	0.57	22.64	96.30	0.19	3.07	0.29
$\triangle SWV_{max}(t2)$	0.68	81.13	48.15	0.29	44.72	< 0.01
$\triangle SWV_{max}(t3)$	0.73	52.83	88.89	0.42	26.21	< 0.01
$\triangle SWV_{max}(t4)$	0.78	52.83	92.59	0.45	38.12	< 0.01
$\triangle SWV_{mean}(t1)$	0.60	22.64	100.00	0.23	1.71	0.15
$\triangle SWV_{mean}(t2)$	0.68	37.74	96.30	0.34	12.02	< 0.01
$\triangle SWV_{mean}(t3)$	0.78	54.72	96.30	0.51	26.21	< 0.01
$\triangle SWV_{mean}(t4)$	0.79	54.72	88.89	0.44	38.88	< 0.01
$\triangle A_{E/B}(t1)$	0.67	67.92	70.37	0.38	12.10	0.02
$\triangle A_{E/B}(t2)$	0.83	77.36	88.89	0.66	18.73	< 0.01
$\triangle A_{E/B}(t3)$	0.78	92.45	55.56	0.48	52.69	< 0.01
$\triangle A_{E/B}(t4)$	0.79	83.02	66.67	0.50	51.11	< 0.01
$\triangle D_{MRI}(t4)$	0.55	37.50	81.82	0.19	0.16	0.62

Abbreviation: AUC, area under curve; D_{US}, longest diameter of tumor in the greyscale US; SWV_{max}, the maximum shear wave velocity; SWV_{mean}, the average shear wave velocity; $A_{E/B,}$ area ratio of lesion on the shear wave time map to the B-mode US screen; D_{MRI}, longest diameter of tumor on the MR image.

Predictive diagnostic performance of combined parameters

According to the results of univariate analysis, variables with statistical significance for predicting the chemotherapy response after each cycle of NAC (after the first NAC cycle: molecular subtype and $\triangle A_{E/B}$; after the second, third and fourth NAC cycles: molecular subtype, $\triangle A_{E/B,}$ $\triangle SWV_{mean}$ and $\triangle SWV_{max}$) were involved in the multivariate logistic regression predictive model.

After completing the screening of variables for the multivariate logistic regression model, only the molecular subtype was identified as a variable capable of predicting the chemotherapy response after the first cycle of NAC (CP1: molecular subtype alone; AUC = 0.83, $p < 0.01$). After the second cycle of NAC, the combination of the molecular subtype and $\triangle A_{E/B}$ was statistically significant for predicting the response to NAC (CP2: molecular subtype and $\triangle A_{E/B}$; AUC = 0.92, $p < 0.01$). Finally, the combination of the molecular subtype, $\triangle A_{E/B,}$ and $\triangle SWV_{mean}$ after the third and fourth cycles of NAC was regarded as a new statistically significant predictor for NAC response (CP3 and CP4: molecular subtype, $\triangle A_{E/B}$ and $\triangle SWV_{mean}$; AUC = 0.94, $p < 0.01$).

The performance of the combined parameters for predicting the response to NAC after each chemotherapy cycle is summarized in Table 5. The sensitivity for predicting the chemotherapy response was only 66.04% after the first NAC cycle, which only depends on the molecular subtype. Furthermore, by adding $\triangle A_{E/B}$, the sensitivity of the combined parameters increased to 86.79% with a specificity of 85.19% after the second cycle of NAC. The combination of the molecular subtype and $\triangle A_{E/B}$ after the second cycle of NAC had better performance for an association of the pathological response to NAC than the variable (molecular subtype) selected after the first cycle of NAC. The molecular subtype combined with $\triangle A_{E/B}$ and $\triangle SWV_{mean}$ had statistically significantly better predictive performance for a response to NAC after the third and fourth cycles of chemotherapy than the variable (molecular subtype) selected after the first cycle of NAC ($\triangle$AUC = 0.11, $p < 0.01$). ROC curves for the combined parameters after each NAC cycle for predicting the pathological response to chemotherapy are presented in Fig. 4. The AUCs of the combined parameters after each cycle were compared as shown in Table 6.

Table 5
Performance of combined parameters according to multivariate regression model for predicting response to NAC

Combined parameters after each cycle of NAC	AUC	Sensitivity(%)	Specificity(%)	Youden index	Cut-off value	*p* value
CP1 (Molecular subtype)	0.83	66.04	96.30	0.62	0.50	< 0.01
CP2 (Molecular subtype&$\triangle A_{E/B}$)	0.92	86.79	85.19	0.72	0.44	< 0.01
CP3 (Molecular subtype&$\triangle A_{E/B}$ &$\triangle SWV_{mean}$)	0.94	86.79	92.59	0.79	0.58	< 0.01
CP4 (Molecular subtype&$\triangle A_{E/B}$ &$\triangle SWV_{mean}$)	0.94	81.13	96.30	0.77	0.74	< 0.01

Abbreviation: AUC, area under curve; CP, combined parameters; $A_{E/B,}$ area ratio of lesion on the shear wave time map to the B-mode US screen; SWV_{mean}; the average shear wave velocity

Table 6
Comparison of AUCs of combined parameters after each cycle of NAC

Comparison of combined parameters	Difference in AUC	*p* value
CP1 vs. CP2	0.09	0.03
CP1 vs. CP3	0.10	< 0.01
CP1 vs. CP4	0.10	< 0.01
CP2 vs. CP3	0.01	0.52
CP2 vs. CP4	0.02	0.53
CP3 vs. CP4	0.00	0.93

Abbreviation: AUC, area under curve; CP, combined parameters

Discussion

The present study was performed to develop a method to reduce the application of unnecessary chemotherapies in poor responders to avoid severe adverse effects from chemotherapy and guide the

selection of an appropriate alternative regimen. The results suggested that SWE can be an early predictor of the pathological response to NAC for breast cancer. The combination of SWE and molecular subtype may be a preferred method for the clinical evaluation of chemotherapy to facilitate the personalization of treatment regimens for breast cancer.

Tumor stiffness obtained with UE, an important biomechanical characteristic, is associated with tumorigenesis and disease progression. Previous experimental studies have revealed that tissue stiffness can be modulated by the extracellular matrix, regulating the proliferation of tumors.[19 20] The composition of the extracellular microenvironment of cancer cells plays a vital role in the breast cancer response to NAC. Higher matrix hardness can increase the risk of chemotherapy resistance.[19] Therefore, as an emerging modality for predominantly representing extracellular matrix features, UE is believed to reflect the microstructural organization of tissues and has the potential to help differentiate a good response to NAC from a poor response.

Compared to SE, SWE provides a more reproducible and quantitative approach for assessing the stiffness of breast lesions.[34] In recent years, the applications and research for SWE in the breast have focused on the diagnosis of breast lesions by assessing the stiffness of tissue.[18] As an emerging and rapidly developing approach to assessing stiffness, SWE has been studied recently for the identification of clinical and pathological responses to NAC and has shown great promise in assessing the chemotherapy response in patients with breast cancer. Our study also showed that SWE has an excellent performance in predicting the NAC pathological response in breast cancer patients, similar to those in previous publications[21 35–41]. Furthermore, our study demonstrated that changes in the number of tumor cells and stromal components reflected by SWE can indicate the breast cancer response to NAC earlier than morphological changes reflected by conventional imaging means.

Some scholars believe that NAC's effectiveness for breast cancer is related to various factors, and a single indicator is inadequate to judge the response to NAC.[38 42 43] Although SWE provides a benefit for the identification of non-responsive cases, but does not significantly improve performance for predicting responders if it is solely used.[44] It has been demonstrated that various breast cancer subtypes differ significantly in the chemotherapy response.[45] Therefore, biological features are usually combined with the clinical characteristics of patients with breast cancer to predict the response to NAC.[46 47] Our study also indicated that the molecular subtype is the most significant factor related to the NAC response among the clinical and pathological characteristics of the patient at the baseline. After the second cycle of NAC, a combination of the molecular subtype and $\triangle A_{E/B}$ was regarded as statistically significant for the prediction of the response to NAC, with significantly higher sensitivity. And previous study also proved that SWE is superior in sensitivity compared to standard clinical assessment or dynamic optical breast imaging, highlighting the potential of SWE to protect patients with chemotherapy resistance from unnecessary NAC.[44 48] Moreover, the combination of molecular subtype, $\triangle A_{E/B}$ and $\triangle SWV_{mean}$, achieved larger AUCs after the third and the fourth cycles of NAC compared to the molecular subtype alone. In

summary, our results showed that elastic and molecular characteristics can be combined to improve the performance for predicting the response to NAC.

Our study revealed that SWE has better potential to predict the pathological response to NAC in breast cancer patients compared to conventional imaging modalities. The combination of the molecular subtype and $\triangle A_{E/B}$ could predict the NAC response with excellent performance after the second cycle of chemotherapy. Early evaluation of the response after two cycles of NAC could provide reliable information about chemotherapy resistance. Moreover, a previous study was performed in an attempt to overcome chemotherapy resistance.[49] The results of our study agreed with previous investigations on the same topic, indicating the potential of SWE for predicting the pathological response to NAC.

Furthermore, a decrease in the longest diameter of tumor evaluated routinely in clinical application using conventional imaging means has not achieved satisfactory outcomes in predicting response to NAC. After NAC, tumor cells become hypoxic and fragment leaving fibrotic and collagenous tissues, which may keep the diameter of tumor unchanged while the volume reduce considerably. When tumor respond to NAC, decrease in tumour cells and changes in extracellular matrix will appear, which could be reflected by UE.[50] Thus, this study focused on early assessment of the response to NAC based on relative changes in the both morphological and biomechanical characteristics of the tumor. Most of previous works exclusively investigated UE features at baseline or before surgery.[21 35 36 39 44] To our knowledge, this study is the first work to assess and compare the performance of SWE, conventional US and MRI for differentiating the response to NAC in the early course of chemotherapy. Further, it is the first attempt to assess the performance of the combination of SWE and molecular subtype in predicting the NAC response, which is less-cost, non-invasive and more accessible with enormous potential clinical and economic benefits.

However, several limitations were present in the study. The first limitation is the unavoidable bias due to the small sample size and the observational study design in a single research center. Large-scale randomized controlled trials are needed to confirm our findings in the future. Next, we did not have enough data to perform subgroup analysis on the specific molecular type of breast cancer due to the limited sample size. Finally, SWE should be performed on axillary lymph nodes to provide more information regarding the response to NAC. Further research on SWE is warranted to achieve more practical applications and identify broader prospects for assessing and predicting the responses to NAC for breast cancer.

Conclusion

In summary, SWE could be used for the early assessment and prediction of the pathological response to NAC for breast cancer. Our findings highlight the potential utility of the combination SWE with molecular subtype to early provide useful information on response to NAC for clinical decision-making.

Declarations

Acknowledgments

The authors would like to thank all the involved study investigators for dedicating their time and skills to the completion of this study. The authors would also like to thank Medjaden Bioscience Limited for assistance in the preparation of the manuscript.

Authors' Contributions

XQP conceived and designed the project. JXH and SYL collected and interpreted radiological data. JXH drafted the manuscript. YO and CGS prepared the figures and tables. YZ and MJW provided statistical analysis. XQP critically reviewed the manuscript for important intellectual content. All authors read and approved the final manuscript.

Availability of data and materials

Data used for this analysis are available upon reasonable request to the corresponding author.

Ethics approval and consent to participate

The study's design and protocol were approved by the ethics committee of the institutional review board at the Cancer Center of Sun Yat-Sen University (approval GZR2017-047). Written informed consent for study participation and data collection were obtained from all patients.

Consent for publication

Consent for publication was obtained from the person whose data was contained in this manuscript.

Competing interests

The authors declare that they have no competing interests.

Funding information

This work was supported by Science and Technology Project Funds of Guangzhou（N0. 1563000308).

References

1. Bray F, Ferlay J, Soerjomataram I, et al. Global cancer statistics 2018: GLOBOCAN estimates of incidence and mortality worldwide for 36 cancers in 185 countries. CA Cancer J Clin. 2018;68(6):394–424. doi: 10.3322/caac.21492 [published Online First: 2018/09/13].
2. Teshome M, Hunt KK. Neoadjuvant therapy in the treatment of breast cancer. Surgical Oncology Clinics. 2014;23(3):505–23.
3. Mieog J, Van der Hage J, Van De Velde C. Neoadjuvant chemotherapy for operable breast cancer. Br J Surg. 2007;94(10):1189–200.

4. Maur M, Guarneri V, Frassoldati A, et al. Primary systemic therapy in operable breast cancer: clinical data and biological fall-out. Ann Oncol. 2006;17(Suppl 5):v158–64. doi:10.1093/annonc/mdj973 [published Online First: 2006/06/30].
5. Croshaw R, Shapiro-Wright H, Svensson E, et al. Accuracy of clinical examination, digital mammogram, ultrasound, and MRI in determining postneoadjuvant pathologic tumor response in operable breast cancer patients. Ann Surg Oncol. 2011;18(11):3160–3. doi:10.1245/s10434-011-1919-5 [published Online First: 2011/09/29].
6. Chagpar AB, Middleton LP, Sahin AA, et al. Accuracy of physical examination, ultrasonography, and mammography in predicting residual pathologic tumor size in patients treated with neoadjuvant chemotherapy. Ann Surg. 2006;243(2):257–64. doi:10.1097/01.sla.0000197714.14318.6f [published Online First: 2006/01/25].
7. Keune JD, Jeffe DB, Schootman M, et al. Accuracy of ultrasonography and mammography in predicting pathologic response after neoadjuvant chemotherapy for breast cancer. Am J Surg. 2010;199(4):477–84. doi:10.1016/j.amjsurg.2009.03.012 [published Online First: 2010/04/03].
8. Lobbes MB, Prevos R, Smidt M, et al. The role of magnetic resonance imaging in assessing residual disease and pathologic complete response in breast cancer patients receiving neoadjuvant chemotherapy: a systematic review. Insights Imaging. 2013;4(2):163–75. doi:10.1007/s13244-013-0219-y [published Online First: 2013/01/30].
9. Wu LM, Hu JN, Gu HY, et al. Can diffusion-weighted MR imaging and contrast-enhanced MR imaging precisely evaluate and predict pathological response to neoadjuvant chemotherapy in patients with breast cancer? Breast Cancer Res Treat. 2012;135(1):17–28. doi: 10.1007/s10549-012-2033-5 [published Online First: 2012/04/06].
10. Marinovich ML, Houssami N, Macaskill P, et al. Meta-analysis of magnetic resonance imaging in detecting residual breast cancer after neoadjuvant therapy. J Natl Cancer Inst. 2013;105(5):321–33. doi:10.1093/jnci/djs528 [published Online First: 2013/01/09].
11. Sheikhbahaei S, Trahan TJ, Xiao J, et al. FDG-PET/CT and MRI for Evaluation of Pathologic Response to Neoadjuvant Chemotherapy in Patients with Breast Cancer: A Meta-Analysis of Diagnostic Accuracy Studies. Oncologist. 2016;21(8):931–9. doi:10.1634/theoncologist.2015-0353 [published Online First: 2016/07/13].
12. Cao X, Xue J, Zhao B. Potential application value of contrast-enhanced ultrasound in neoadjuvant chemotherapy of breast cancer. Ultrasound Med Biol. 2012;38(12):2065–71. doi:10.1016/j.ultrasmedbio.2012.07.027 [published Online First: 2012/10/16].
13. Corcioni B, Santilli L, Quercia S, et al. Contrast-enhanced US and MRI for assessing the response of breast cancer to neoadjuvant chemotherapy. J Ultrasound. 2008;11(4):143–50. doi:10.1016/j.jus.2008.09.007 [published Online First: 2008/12/01].
14. Chinese anti-cancer association. Experts consensus of breast cancer neoadjuvant therapy in China (version 2019). China Oncology. 2019;29:390e400. [in Chinese).

15. Vriens BE, de Vries B, Lobbes MB, et al. Ultrasound is at least as good as magnetic resonance imaging in predicting tumour size post-neoadjuvant chemotherapy in breast cancer. Eur J Cancer. 2016;52:67–76. doi:10.1016/j.ejca.2015.10.010 [published Online First: 2015/12/10].
16. Lee MC, Gonzalez SJ, Lin H, et al. Prospective trial of breast MRI versus 2D and 3D ultrasound for evaluation of response to neoadjuvant chemotherapy. Ann Surg Oncol. 2015;22(9):2888–94. doi:10.1245/s10434-014-4357-3 [published Online First: 2015/01/16].
17. Forte AJ, Huayllani MT, Boczar D, et al. The basics of ultrasound elastography for diagnosis, assessment, and staging breast cancer-related lymphedema: a systematic review of the literature. Gland Surg. 2020;9(2):589–95. doi:10.21037/gs.2020.02.08 [published Online First: 2020/05/19].
18. Barr RG, Nakashima K, Amy D, et al. WFUMB guidelines and recommendations for clinical use of ultrasound elastography: Part 2: breast. Ultrasound Med Biol. 2015;41(5):1148–60. doi:10.1016/j.ultrasmedbio.2015.03.008 [published Online First: 2015/03/22].
19. Schrader J, Gordon-Walker TT, Aucott RL, et al. Matrix stiffness modulates proliferation, chemotherapeutic response, and dormancy in hepatocellular carcinoma cells. Hepatology. 2011;53(4):1192–205. doi:10.1002/hep.24108 [published Online First: 2011/03/29].
20. Oskarsson T. Extracellular matrix components in breast cancer progression and metastasis. Breast. 2013;22(Suppl 2):66–72. doi:10.1016/j.breast.2013.07.012 [published Online First: 2013/10/01].
21. Ma Y, Zhang S, Li J, et al. Comparison of strain and shear-wave ultrasounic elastography in predicting the pathological response to neoadjuvant chemotherapy in breast cancers. Eur Radiol. 2017;27(6):2282–91. doi:10.1007/s00330-016-4619-5 [published Online First: 2016/10/19].
22. Deffieux T, Gennisson JL, Bercoff J, et al. On the effects of reflected waves in transient shear wave elastography. IEEE Trans Ultrason Ferroelectr Freq Control. 2011;58(10):2032–5. doi:10.1109/tuffc.2011.2052 [published Online First: 2011/10/13].
23. Therasse P, Arbuck SG, Eisenhauer EA, et al. New guidelines to evaluate the response to treatment in solid tumors. European Organization for Research and Treatment of Cancer, National Cancer Institute of the United States, National Cancer Institute of Canada. J Natl Cancer Inst. 2000;92(3):205–16. doi:10.1093/jnci/92.3.205 [published Online First: 2000/02/03].
24. AIUM practice guideline for the. performance of a breast ultrasound examination. J Ultrasound Med. 2009;28(1):105–9. doi:10.7863/jum.2009.28.1.105 [published Online First: 2008/12/25].
25. Sun CY, Lei KR, Liu BJ, et al. Virtual touch tissue imaging and quantification (VTIQ) in the evaluation of thyroid nodules: the associated factors leading to misdiagnosis. Sci Rep. 2017;7:41958. doi:10.1038/srep41958 [published Online First: 2017/02/06].
26. Sauter G, Lee J, Bartlett JM, et al. Guidelines for human epidermal growth factor receptor 2 testing: biologic and methodologic considerations. J Clin Oncol. 2009;27(8):1323–33. doi:10.1200/jco.2007.14.8197 [published Online First: 2009/02/11].
27. Goldhirsch A, Winer EP, Coates AS, et al. Personalizing the treatment of women with early breast cancer: highlights of the St Gallen International Expert Consensus on the Primary Therapy of Early

Breast Cancer 2013. Ann Oncol. 2013;24(9):2206–23. doi:10.1093/annonc/mdt303 [published Online First: 2013/08/07].

28. Cheang MC, Chia SK, Voduc D, et al. Ki67 index, HER2 status, and prognosis of patients with luminal B breast cancer. J Natl Cancer Inst. 2009;101(10):736–50. doi:10.1093/jnci/djp082 [published Online First: 2009/05/14].
29. Howlader N, Altekruse SF, Li CI, et al. US incidence of breast cancer subtypes defined by joint hormone receptor and HER2 status. J Natl Cancer Inst 2014;106(5) doi:10.1093/jnci/dju055 [published Online First: 2014/04/30].
30. Voduc KD, Cheang MC, Tyldesley S, et al. Breast cancer subtypes and the risk of local and regional relapse. J Clin Oncol. 2010;28(10):1684–91. doi:10.1200/jco.2009.24.9284 [published Online First: 2010/03/03].
31. Ogston KN, Miller ID, Payne S, et al. A new histological grading system to assess response of breast cancers to primary chemotherapy: prognostic significance and survival. Breast. 2003;12(5):320–7. doi:10.1016/s0960-9776(03)00106-1 [published Online First: 2003/12/09].
32. Hajian-Tilaki K. Receiver Operating Characteristic (ROC) Curve Analysis for Medical Diagnostic Test Evaluation. Caspian J Intern Med. 2013;4(2):627–35.
33. Ruopp MD, Perkins NJ, Whitcomb BW, et al. Youden Index and optimal cut-point estimated from observations affected by a lower limit of detection. Biom J. 2008;50(3):419–30. doi:10.1002/bimj.200710415.
34. Cosgrove DO, Berg WA, Doré CJ, et al. Shear wave elastography for breast masses is highly reproducible. Eur Radiol. 2012;22(5):1023–32. doi:10.1007/s00330-011-2340-y [published Online First: 2012/01/03].
35. Evans A, Armstrong S, Whelehan P, et al. Can shear-wave elastography predict response to neoadjuvant chemotherapy in women with invasive breast cancer? Br J Cancer. 2013;109(11):2798–802. doi:10.1038/bjc.2013.660 [published Online First: 2013/10/31].
36. Lee SH, Chang JM, Han W, et al. Shear-Wave Elastography for the Detection of Residual Breast Cancer After Neoadjuvant Chemotherapy. Ann Surg Oncol. 2015;22(Suppl 3):376-84. doi:10.1245/s10434-015-4828-1 [published Online First: 2015/08/25].
37. Evans A, Whelehan P, Thompson A, et al. Prediction of Pathological Complete Response to Neoadjuvant Chemotherapy for Primary Breast Cancer Comparing Interim Ultrasound, Shear Wave Elastography and MRI. Ultraschall Med. 2018;39(4):422–31. doi:10.1055/s-0043-111589 [published Online First: 2017/09/22].
38. Ma Y, Zhang S, Zang L, et al. Combination of shear wave elastography and Ki-67 index as a novel predictive modality for the pathological response to neoadjuvant chemotherapy in patients with invasive breast cancer. Eur J Cancer. 2016;69:86–101.
39. Fernandes J, Sannachi L, Tran WT, et al. Monitoring Breast Cancer Response to Neoadjuvant Chemotherapy Using Ultrasound Strain Elastography. Transl Oncol. 2019;12(9):1177–84. doi:10.1016/j.tranon.2019.05.004 [published Online First: 2019/06/22].

40. Jing H, Cheng W, Li ZY, et al. Early Evaluation of Relative Changes in Tumor Stiffness by Shear Wave Elastography Predicts the Response to Neoadjuvant Chemotherapy in Patients With Breast Cancer. J Ultrasound Med. 2016;35(8):1619–27. doi:10.7863/ultra.15.08052 [published Online First: 2016/06/16].
41. Evans A, Whelehan P, Thompson A, et al. Identification of pathological complete response after neoadjuvant chemotherapy for breast cancer: comparison of greyscale ultrasound, shear wave elastography, and MRI. Clin Radiol. 2018;73(10):910.e.
1-10.e6
. doi: 10.1016/j.crad.2018.05.030 [published Online First: 2018/07/08].
42. Firouzabadi D, Rezvani A, Dehghanian A, et al. Association of ki67 and tumor marker p53 in locally advanced breast cancer patients and evaluation of response to neoadjuvant chemotherapy: a survey in South Iran. Cancer Manag Res. 2019;11:6489–97. doi:10.2147/CMAR.S203831.
43. Zhang J, Gao S, Zheng Q, et al. A Novel Model Incorporating Tumor Stiffness, Blood Flow Characteristics, and Ki-67 Expression to Predict Responses After Neoadjuvant Chemotherapy in Breast Cancer. Front Oncol. 2020;10:603574.
44. Maier AM, Heil J, Harcos A, et al. Prediction of pathological complete response in breast cancer patients during neoadjuvant chemotherapy: Is shear wave elastography a useful tool in clinical routine. Eur J Radiol. 2020;128:109025.
45. Yang TJ, Morrow M, Modi S, et al. The Effect of Molecular Subtype and Residual Disease on Locoregional Recurrence in Breast Cancer Patients Treated with Neoadjuvant Chemotherapy and Postmastectomy Radiation. Ann Surg Oncol. 2015;22(Suppl 3):495–501. doi:10.1245/s10434-015-4697-7 [published Online First: 2015/07/02]. Suppl 3) .
46. Brenton JD, Carey LA, Ahmed AA, et al. Molecular classification and molecular forecasting of breast cancer: ready for clinical application? J Clin Oncol. 2005;23(29):7350–60. doi:10.1200/jco.2005.03.3845 [published Online First: 2005/09/08].
47. von Minckwitz G, Untch M, Blohmer JU, et al. Definition and impact of pathologic complete response on prognosis after neoadjuvant chemotherapy in various intrinsic breast cancer subtypes. J Clin Oncol. 2012;30(15):1796–804. doi:10.1200/jco.2011.38.8595 [published Online First: 2012/04/18].
48. Zhang J, Tan X, Zhang X, et al. Efficacy of shear-wave elastography versus dynamic optical breast imaging for predicting the pathological response to neoadjuvant chemotherapy in breast cancer. Eur J Radiol. 2020;129:109098.
49. von Minckwitz G, Blohmer JU, Costa SD, et al. Response-guided neoadjuvant chemotherapy for breast cancer. J Clin Oncol. 2013;31(29):3623–30. doi:10.1200/jco.2012.45.0940 [published Online First: 2013/09/05].
50. Wang JW, Guo ZX, Lin QG, et al. Ultrasound elastography as an imaging biomarker for detection of early tumor response to chemotherapy in a murine breast cancer model: a feasibility study. Br J Radiol. 2018;91(1085):20170698.

Figures

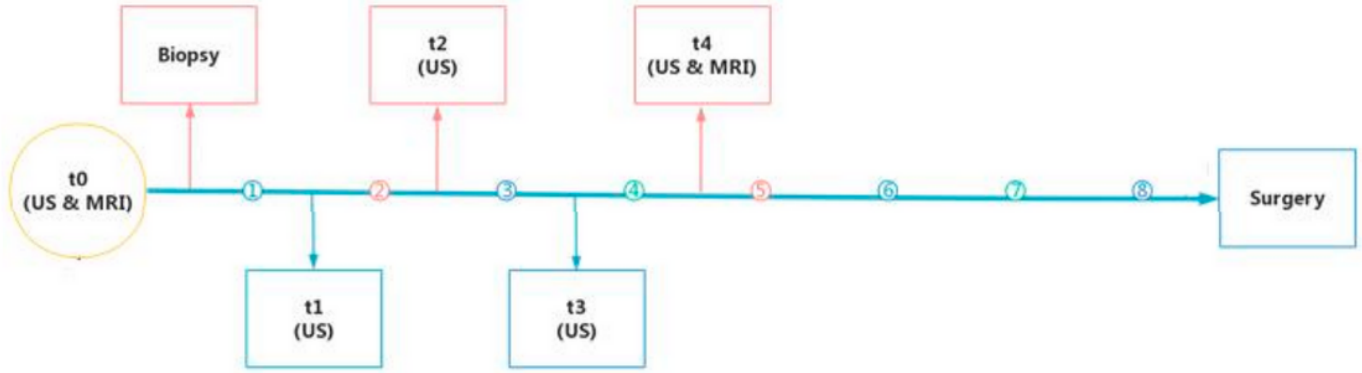

Figure 1

Flow chart depicting the study design with imaging examination in ultrasonography (US) and magnetic resonance imaging (MRI)

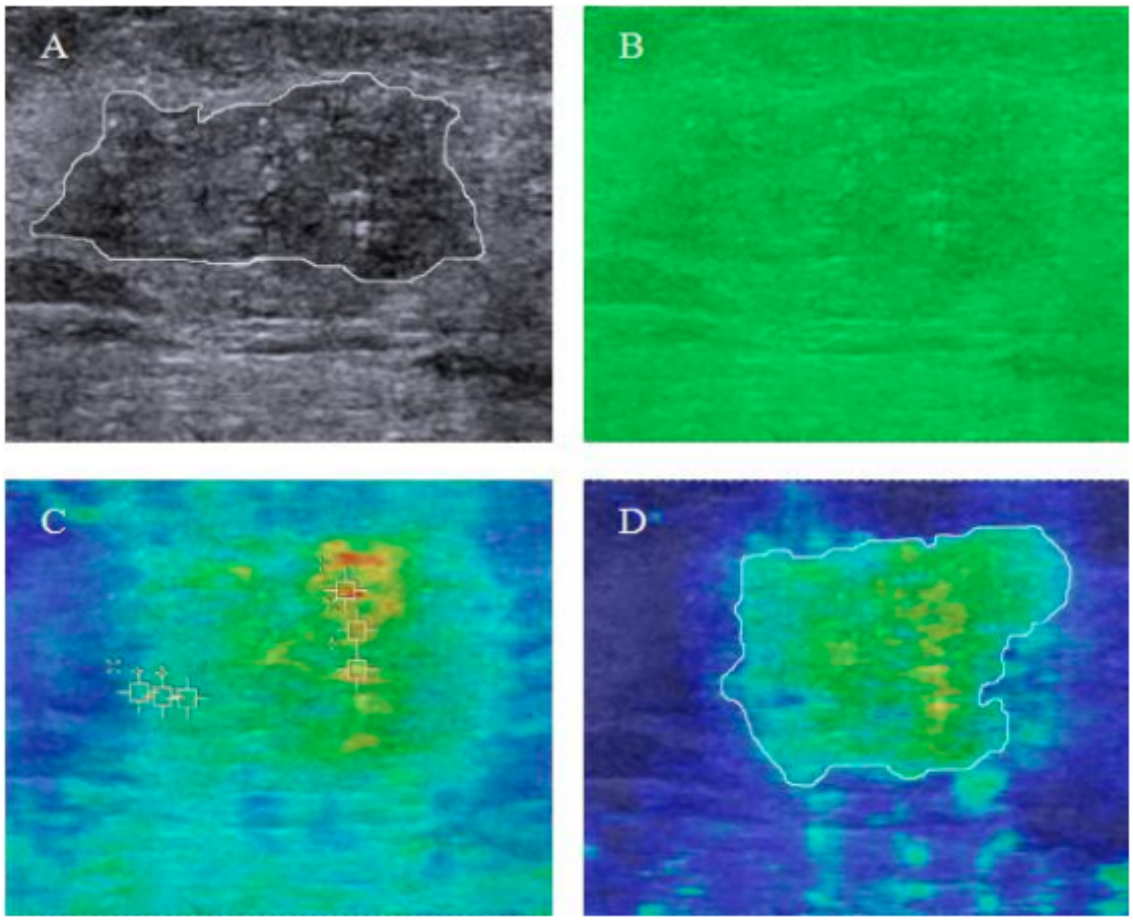

Figure 2

Images of ultrasound and shear wave elastography (SWE) examination. (A) Ultrasonic gray-scale image of breast cancer lesions. (B) Quality map of quantitative SWE. (C) Velocity diagram of quantitative SWE (The maximum and minimum shear wave acquired in the hardest and softest regions with high imaging quality, respectively). (D) Time map of quantitative SWE (The profile of the breast lesion traced and the area of the lesion measured on the ultrasonic machine according to the color-coded differences between the lesion and the surrounding tissues).

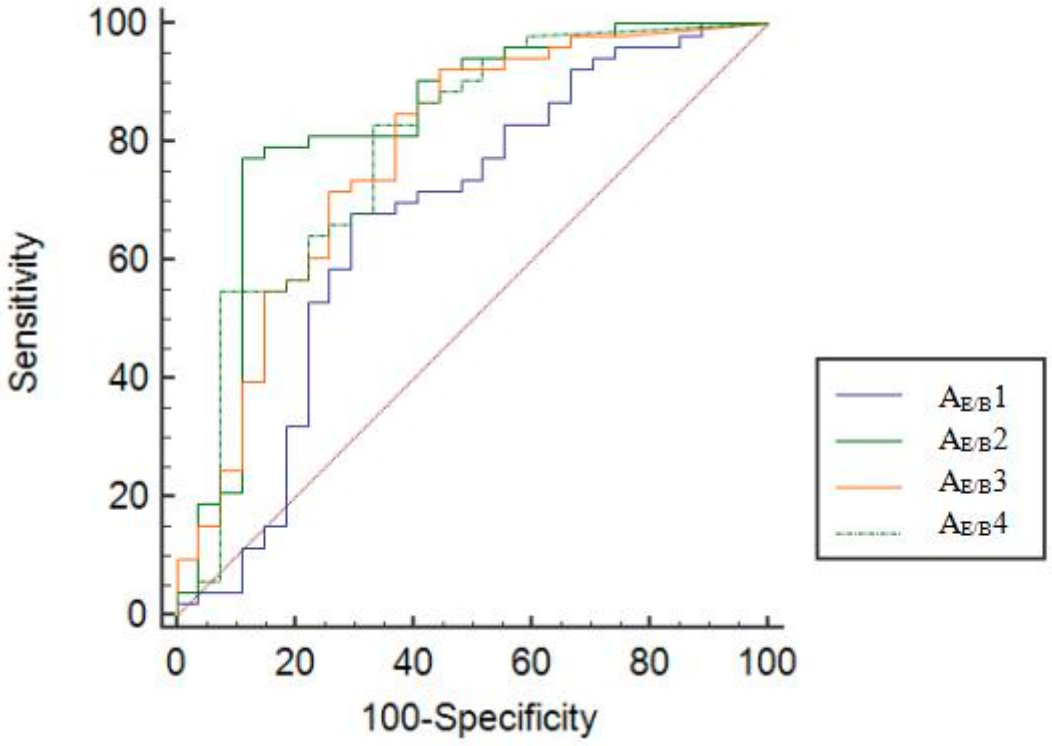

Figure 3

The ROC curve of △AE/B in distinguishing pathological response during the early stages of NAC

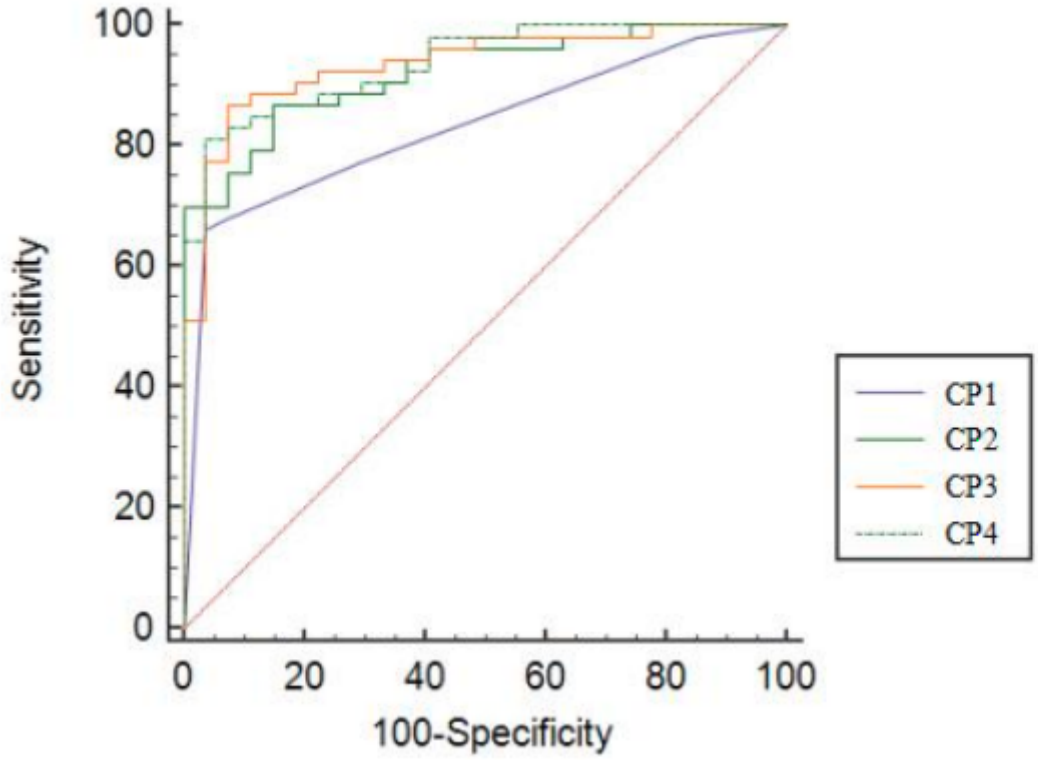

Figure 4

The ROC of combined parameters after first, second, third, and fourth cycles of NAC (t1-t4).

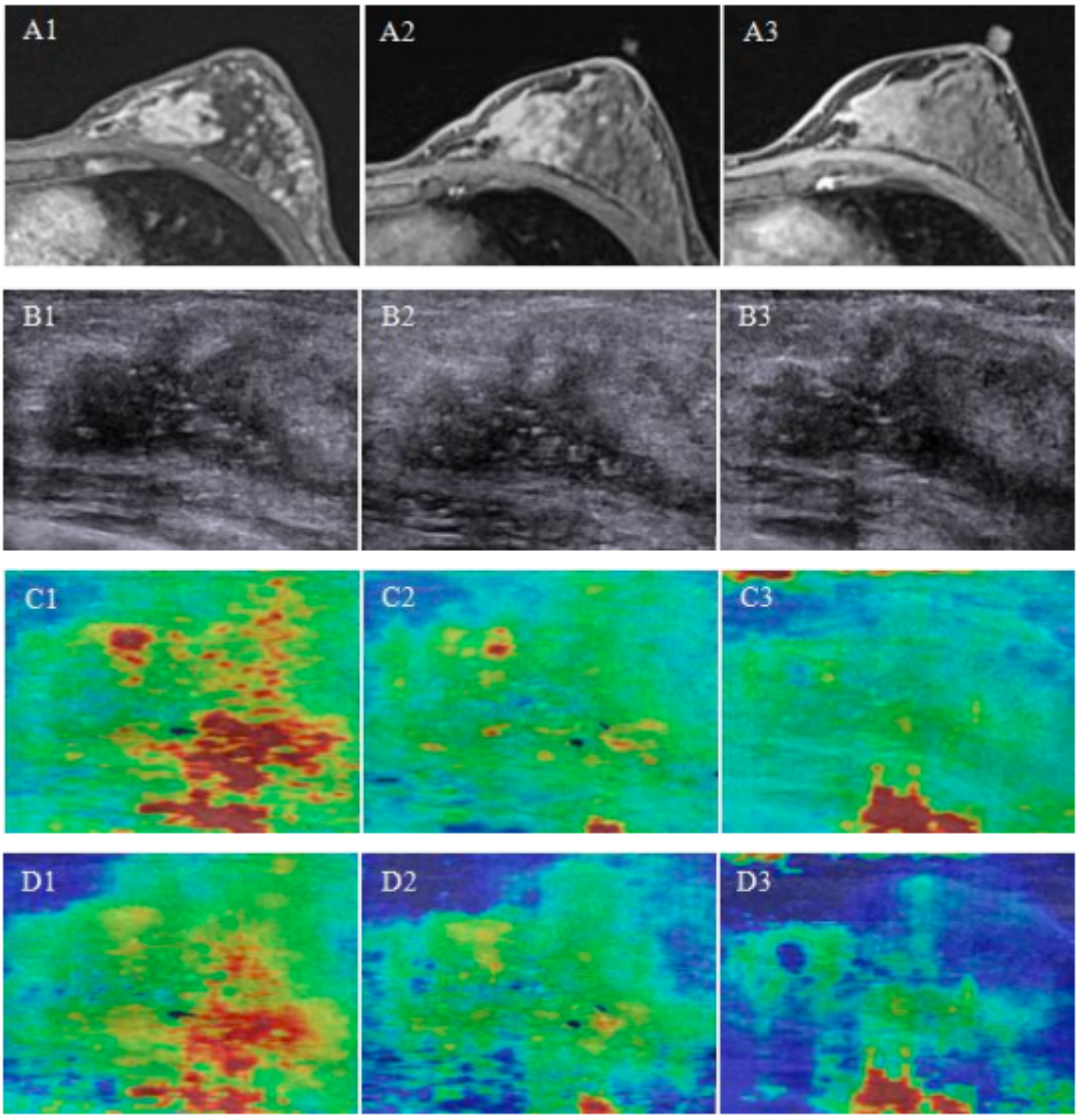

Figure 5

The representative dynamic changes of breast lesion on MRI, B-mode ultrasound, and SWE maps The patient was a 45-year-old woman with luminal B2 breast cancer shown on the left, and the postoperative pathologic evaluation was 4 points. A1-A3 show the breast CE-MR images before NAC, after the fourth course of chemotherapy, and before surgery; B1-B3 show the B-mode ultrasound images of the breast tumor before the beginning of NAC and after the second and fourth courses of chemotherapy. C1-C3 show the shear wave velocity diagram of the breast tumor before the beginning of NAC and after the second and fourth courses of chemotherapy. D1-D3 show the shear wave time graph for the breast tumor before the onset of NAC and after the second and fourth courses of chemotherapy. SWVmax(t0) = 9.54 m/s, SWVmax(t2) = 6.83 m/s, SWVmax(t4) = 4.33 m/s; SWVmean(t0) = 6.52 m/s, SWVmean(t2) = 4.65 m/s, SWVmean(t4) = 3.48 m/s; AE/B(t0) = 1.48, AE/B(t2) = 1.04, AE/B(t4) = 0.69

Supplementary Files

This is a list of supplementary files associated with this preprint. Click to download.

- Appendixes.pdf